Submitted to PNAS (8/24/2018**), Classification:** Physical - Earth

Earthquake Swarms and Slow Slip on a Sliver Fault in the Mexican Subduction Zone

Shannon Fasola[a]
Michael R. Brudzinski [a]
Stephen G. Holtkamp [b]
Shannon E. Graham [c]
Enrique Cabral-Cano [d]

[a] Department of Geology and Environmental Earth Science, Miami University, Oxford, OH
[b] Geophysical Institute, University of Alaska-Fairbanks, Fairbanks, AK
[c] Department of Earth and Environmental Sciences, Boston College, Chestnut Hill, MA
[d] Instituto de Geofísica, Universidad Nacional Autónoma de México. Ciudad Universitaria, Delegación Coyoacán, C.P. 04510, CDMX, México.

Corresponding Author:
Shannon Fasola: fasolasl@miamioh.edu

Keywords: swarm seismicity, slow slip, sliver faults, subduction zone, Mexico

ABSTRACT

The Mexican Subduction Zone is an ideal location for studying subduction processes due to the short trench-to-coast distances that bring broad portions of the seismogenic and transition zones of the plate interface inland. Using a recently generated seismicity catalog from a local network in Oaxaca, we identified 20 swarms of earthquakes (M<5) from 2006-2012. Swarms outline what appears to be a steeply dipping structure in the overriding plate, indicative of an origin other than the plate interface. This steeply dipping structure corresponds to the northern boundary of the Xolapa terrane. In addition, we observed a new characteristic of slow slip events (SSEs) where they showed a shift from trenchward motion towards an along-strike direction at coastal GPS sites. A majority of the swarms were found to correspond in time to the along-strike shift. We propose that swarms and SSEs are occurring on a sliver fault that allows the oblique convergence to be partitioned into trench perpendicular motion on the subduction interface and trench parallel motion on the sliver fault. The resistivity structure surrounding the sliver fault suggests that SSEs and swarms of earthquakes occur due to high fluid content in the fault zone. We propose that the sliver fault provides a natural pathway for buoyant fluids attempting to migrate upward after being released from the downgoing plate. Thus, sliver faults could be responsible for the downdip end of the seismogenic zone by creating drier conditions on the subduction interface trenchward of the sliver fault, promoting fast-slip seismogenic rupture behavior.

Significance Statement

We provide a new interpretation for the interaction of crustal faults, clusters of earthquakes (swarms), and slow slip (a slower form of fault rupture) in southern Mexico. Our observations indicate that swarms and slow slip are occurring on a sliver fault in the overriding plate that allows the oblique plate convergence to be separated into a trench perpendicular and parallel motion on the subduction interface and sliver fault, respectively. We propose the sliver fault provides a natural pathway for buoyant fluids attempting to migrate upward after being released from the downgoing plate. Thus, sliver faults could be responsible for the downdip end of the seismogenic zone by creating drier conditions on the subduction interface trenchward of the sliver fault.

1. Introduction

Many of the world's most devastating earthquakes have been ruptures of the seismogenic zone along the subduction interface (1), highlighting the importance of studying fault slip in subduction zones. Within the last couple decades, slow slip events (SSEs) have been observed to occur regularly downdip of the seismogenic zone, where there is a transition in frictional behavior from stick-slip to stable sliding, as a way of releasing accumulated strain (2–4). SSEs typically last weeks to months and are often accompanied by tectonic (non-volcanic) tremor that appears to represent a swarm of small, low-frequency earthquakes (2, 5–8). There have also been multiple cases where SSEs have been suggested to promote swarms of traditional earthquakes (9–14). Earthquake swarms are empirically defined as an increase in seismicity rate above the background rate without a clear triggering mainshock, having an abrupt beginning and end, and having several earthquakes of similar magnitudes to the largest magnitude event (15–17). When considered as a single event, swarms have similar durations and cumulative moment to SSEs, as well as similar along-strike propagation velocities (~10 km/day; (18)).

The Mexican Subduction Zone is a natural laboratory for studying these slip processes due to the relatively short (~50 km) trench-to-coast distance that brings broad portions of the seismogenic and transition zones ~250 km inland, providing a chance to pursue detailed studies of the plate interface. A recently developed catalog of seismicity in the Oaxaca region, referred to as the OXNET catalog, has revealed a large amount of inland seismicity, including a band of intense seismicity occurring ~50 km inland from the trench (Fig. 1a)(19). SSEs and tectonic tremor have been well documented further inland from this seismicity band (Fig. 1a)(19, 24–28), suggesting this band marks the frictional transition on the plate interface from velocity weakening to velocity strengthening (6). Other studies have used shallow thrust earthquakes to define the downdip limit of the seismogenic zone in southern Mexico (29–31), and this corresponds with where the seismicity band occurs (Fig. 1a). However, these studies pointed out that the depth of ~25 km is nearly half of the typical depth for most subduction zones (45 +/- 5 km and up to 55 km; (32, 33)).

The narrow seismogenic zone is thought to be a result of the geometry of the subducting plate and the fact that the overriding plate is oceanic in origin and only ~45 km thick, half the lithospheric thickness in South America where the seismogenic zone is almost twice as deep (30, 34). The overriding plate in this region consists of different lithologic terranes, mainly the Mixteco, Oaxaca, and Xolapa terranes (Fig. 1b). In fact, the Xolapa terrane overlies the band of intense seismicity and the Xolapa-Mixteco boundary is consistent with its inland extent. The Xolapa terrane consists of the highly deformed Xolapa Metamorphic Complex, which by some have been proposed to be of accretionary origin, and un-deformed plutonic intrusions (35, 36). Some studies have proposed that faults and shear zones occur along portions of the northern boundary of the Xolapa terrane (22, 35, 37–39). In fact, an interesting characteristic of slip has been observed in the Mexican Subduction Zone, where coastal GPS sites have shown a small but significant along-strike motion during the trenchward motion of SSEs (24, 40, 41) inferring slip on crustal faults in the overriding plate.

In Mexico, SSEs are associated with an ultra-slow velocity layer (USL) interpreted to represent a fluid-saturated portion of the oceanic crust, forming a high pore-fluid pressure layer (42). The high pore-fluid pressures of the USL would be expected to greatly reduce the effective normal stress on the plate interface, promoting episodic slow slip (43, 44) and dynamic triggering of tectonic tremor (45). The fate of fluids trenchward of the USL remains debated. Zones of high conductivity near the coast (Fig. 1b) suggest that fluids are released from the slab updip of the USL (21, 22) which could impact the occurrence of seismicity. In Oaxaca, Colella et al. (46) suggest that trapped fluids in the low-permeability seal along the plate interface (47–49) may be released by SSEs which then flow upwards along the plate interface generating seismicity, as a swarm of earthquakes was found to correspond to a SSE. The migrating fluids would raise pore-fluid pressures and lower the effective stresses over a period of time to promote swarm seismicity. While earthquake swarms are not as well studied in Mexico, the band of intense seismicity below the Xolapa terrane appears in clusters near the downdip edge of the seismogenic zone, indicating swarms may be prevalent (19).

In this study, we aim to better understand the shallow portion of the megathrust as it relates to various slip processes (i.e., seismicity, swarms, and slow slip), upper crustal structures, and fluids. We focus on the Oaxaca region (Fig. 1), where we can utilize the OXNET catalog of local seismicity and continuous GPS (cGPS) network in place (24–26). We seek to identify

swarms of earthquakes, their relationship to SSEs, and whether they occur along the plate interface as in most subduction zones (9–14) or along forearc crustal faults (50–52).

2. Methods

Earthquake swarms are generated from the OXNET catalog of local seismicity which spans from June 2006 to March 2012 and utilizes the local and permanent networks of broadband seismometers (19). Swarms are identified using the swarm-characterization method of Holtkamp and Brudzinski (18). Every burst of seismicity, the apparent line of vertical dots in a magnitude vs. time plot, was inspected for the 3 empirical traits of swarm sequences: no clear triggering mainshock, many events the near the maximum size, and a relatively constant seismicity rate throughout the sequence (Fig. S2). For slow slip comparison with the swarms, GPS data was obtained from 11 cGPS stations in Oaxaca spanning the duration of the OXNET catalog. GPS data were processed with Release 6.1 of the GIPSY software suite from the Jet Propulsion Laboratory (JPL). We did not solve for source locations of SSEs along the plate interface, as a catalog of SSEs in Oaxaca was recently compiled (53) utilizing the same cGPS stations. To better interpret the seismicity and GPS motions, we also reexamined the configuration of the northern boundary of the Xolapa terrane based on the extent of the core complex (36), aeromagnetic data (20), and topographic information (22). See *Supporting Information* section S1 for a more detailed discussion of the methods used in this study.

3. Swarms in Oaxaca

3.1. Characterization

The recently generated OXNET catalog revealed 20 swarms of earthquakes from June 2006 to March 2012 (Table S1.txt), with anywhere from 5 to 50 earthquakes in each cluster and an average of 20. Durations of swarms vary from hours to weeks with two swarms lasting over a month. When considered as a single event, the total seismic moment release for the swarms ranged from 3.8 to 5.3. Individual earthquake magnitudes ranged from 2.5 to 5.0 (Fig. 2).

To confirm that the swarms we have identified follow the patterns of previous studies, we use the quantitative methods first suggested by Vidale and Shearer (54) that examined the relation of the largest event in each swarm and number of events in that swarm (Fig. S4) in addition to the relative timing of events within the swarm (Fig. S5) (see section S2). Even though our swarm catalog is smaller than Vidale and Shearer (54), we still see similar characteristics in our swarms providing evidence that our catalog is in fact swarms.

3.2. Spatial Distribution

Swarms are distributed along the shallow portion of the subduction zone and more or less form a trend parallel to the trench with several large swarms (with M>4.6 earthquakes in 2008, 2010, and 2011) also striking in a roughly trench perpendicular configuration (Fig. 3). Due to the magnitude of events and station configuration, we were not able to determine focal mechanisms for the swarms. We searched the global Centroid Moment Tensor (CMT) catalog and found only one solution for an event in one of the larger swarms that formed a trend perpendicular to the trench with a steeply dipping reverse fault striking NE-SW.

We divided the swarms into a western (a), central (b), and eastern (c) region (Fig. 3) to emphasize an unexpected feature in the central region and the uncertainty in depths with the regions in the west and east. The uncertainty of event locations within the swarms are 5 km

horizontally and 7 km vertically (19). A majority of the swarms occurred between 10–30 km depth, mostly above the megathrust zone as 25 km depth approximately marks the downdip extent of the seismogenic zone in southern Mexico (29–31). Surprisingly, many swarms do not follow the dip of the plate interface, but instead are consistent with a steeply dipping structure ~50–100 km inland from the trench (Fig. 4). Our best constrained locations and depths are in the central region as they have the best station configuration for determining locations. Even with the 7 km uncertainty in depth (19), the uncertainty is not going to dispel the apparent vertical feature as it extends for over 20 km. There are not enough well-determined depths for the eastern and western swarms to determine where they are occurring along the subduction zone, due to their proximity to the edge of our network.

An interesting characteristic of the swarms trending parallel to the trench is that they fall near the northern boundary of the Xolapa terrane (Fig. 3), where Arzate-Flores et al. (22) proposed a regional fault system dipping to the south. Earlier studies marked the terrane boundary as regional shear zones or faults such as the Chacalapa-La Venta left-lateral transtensional and normal ductile shear zone (Fig. 1b) (35, 37–39). We find swarms parallel the northern extent of the Xolapa Complex (36) more than the terrane boundary (Fig. 3). Therefore, we provide a revised boundary for the lithologic terrane based on the extent of the core complex (see section S1.5), which is supported by aeromagnetic data (20) and topographic information (22). We find that seismicity parallels this boundary but is shifted to the south due to the dip of the boundary (Fig. 3). The steeply dipping seismicity feature and refined surface trend of the terrane based on the core complex are both parallel to the trench as well (Fig. 4b). The steeply dipping structure outlined by the swarms and their proximity to the northern extent of the Xolapa Complex suggests swarms may occur on a crustal fault, such as the Chacalapa-La Venta fault. We will henceforth refer to the region south of our refined trajectory as the Xolapa terrane, as we are referring to a section of the plate, primarily composed of the Xolapa Complex, that is moving separately from the mainland along our interpretation of a crustal fault.

3.3. Swarms and SSEs

When comparing the timing of our swarms to SSEs from Graham et al. (53), we see no clear relationship between slow slip and swarms as less than a third of swarms occur during detected SSEs (Fig. 5) which is less than the chance of a random occurrence of SSE and swarms given that SSEs occurred during ~35% of our study. However, given that an along-strike motion has been observed during SSEs on coastal sites in Guerrero (24, 40, 41), we took another look at GPS data in Oaxaca to see if we could observe similar patterns and maybe a new correlation to swarms.

We found that all of the 5 previously-detected SSEs in Oaxaca during our study (2007, 2008-2009, mid-2010, 2010-2011, 2011-2012) showed a shift, in time, from a trenchward dominant motion towards an along-strike dominant motion at coastal GPS sites. We refer to the periods of along-strike dominant motion as along-strike SSEs (a-SSEs). Coastal sites would exhibit along-strike motion towards the southeast (SE), while inland sites displayed along-strike motion towards the northwest (NW) indicating some degree of opposing slip (Fig. 6a). Fig. 5 highlights periods of a-SSEs for each SSE at the best observed coastal station, OXTU. Even though, we cannot see the a-SSE fully at OXTU during the 2007 SSE due to equipment failure, the a-SSE is confirmed at coastal station OXLP. A-SSEs typically lasted ~3-6 months, and differential initiation of the motion at GPS stations suggested slip migration. What is intriguing,

is that the a-SSE appears to be occurring at the same time as the trenchward motion of the SSEs (Fig. 5), indicating there may be some relationship between motion on the plate interface and motion on crustal faults.

In support of our geodetic observations, slip models for each SSE along the plate interface from Graham et al. (53) show isolated patches of slip closer to the coast that correspond to when we observed periods of a-SSEs on the nearest GPS site to the slip patch. These patches of slip were all south of the Xolapa terrane boundary, just as the swarms were, indicating the crustal Chacalapa-La Venta fault may have active strike-slip motion on it. Brudzinski et al. (24) also observed an intriguing feature of slip when characterizing SSEs in Oaxaca where time-series of monthly average locations for GPS sites showed a complicated slip pattern before the 2006 SSE. Data with the steady northeastward strain accumulation removed, show an almost rotational characteristic in the E-W direction.

Surprisingly, each swarm that occurred during a SSE was found to correspond to the period of a-SSE observed at coastal GPS sites rather than to the period of trenchward dominant motion. Those swarms also locate near the modelled slip patches from Graham et al. (53), both of which are near the northern boundary of the Xolapa terrane. The best observed case is the April 2008 - October 2009 SSE and March 10-19, 2009 swarm where the swarm, isolated slip patch, and a GPS site (OXTU) are all in close proximity to each other (Fig. 6a). GPS velocities were estimated from the yellow blocks of time in Fig. 6b for periods of a-SSE with a simple calculation of displacement over time to confirm presence of opposing motion of coastal and inland sites. GPS velocities have steady northeastward strain accumulation and southwestward strain release from the slow slip along the plate interface, both of which were also estimated from a portion of the time-series, removed to accentuate along-strike motion. GPS velocities during the trench perpendicular dominant motion (i.e., typical of SSEs on the plate interface) were also estimated from a portion of the pink blocks of time where there was a constant slope at each station. The steady northeastward strain accumulation was removed. The “corrected” GPS velocities for both coastal site OXTU and inland sites OXGU and OAX2, show a shift from trenchward dominant motion towards along-strike dominant motion oriented to the SE and NW, respectively. A-SSE is first seen at OXPE and OXLP and then at OXTU where the March 2009 swarm occurs near the end of, further indicating slip may have migrated along-strike. Based on the propagation of events within the swarm, we estimated an along-strike migration rate of ~4.6 km/day (Fig. 6c), similar to rates for Oaxaca SSEs (1.5-4 km/day; (53)).

Intriguingly, GPS velocities north of the Xolapa terrane boundary during periods of a-SSE show a change towards the overall plate convergence vector. We would expect the GPS velocities to be less affected by movement along a strike-slip crustal fault the farther away they are. Similarly, the decrease in the sinistral component of GPS velocity as you move inland is seen in Guerrero (55, 56).

Similar observations of the 2008-2009 SSE and March 2009 swarm are seen with the other SSEs and corresponding swarms. The proximity of the swarms to the northern boundary of the Xolapa terrane in addition to our observations of a-SSEs indicate the two may be related. Without a GPS right next to each swarm as is with the March 2009 swarm, it is difficult to determine at what point the swarms occurred during the a-SSE. However, each swarm occurs at some point during the a-SSE (Fig. 5). The only exception is the 2007 SSE case, where hardware failures and other operational problems with GPS sites led to a less complete record of the 2007 SSE than for the other SSEs (53). As a result, we cannot resolve whether there was any

geographic or temporal overlap between the a-SSE and the 2007 swarm given the a-SSE was only observed at OXLP ~70 km and partially at OXTU ~35 km from the swarm which could also indicate along-strike migration of slip assuming the swarm is the first observation of slip. For some cases, two swarms occur, such as for the 2010-2011 and 2011-2012 SSEs (Fig. 5), indicating a larger area could be slipping than what is observed in the 2008-2009 SSE case.

Since less than a third of the swarms show a correlation with a-SSEs, the question arises what is the explanation for the others. These were cases where (a) the along-strike motion is not as prominent as the others indicating a-SSEs may be too-small to be detected, (b) swarms trend perpendicular to the trench and as such would not be expected to show an along-strike motion, (c) swarms occur at the beginning of our study, a time when GPS stations were not as widely installed leading to a lack of nearby stations to determine if they correspond to along-strike motion, and (d) swarms had the shortest (~18 min.) or longest (>45 days) durations such that they would not register a change on GPS sites. However, we do believe that the 3 swarms at the beginning of our study occur on the same structure as the swarms that correlate with a-SSEs, because they too outline a steeply dipping structure in cross-section (Fig. 4b).

4. 2012 Ometepec Afterslip

Given the swarms were found to correspond to a shift from trenchward dominant to along-strike dominant motion near the northern Xolapa terrane boundary, we wondered if the a-SSEs could be observed at other times, in particular, with afterslip associated with large megathrust earthquakes. The Mw=7.4 Ometepec megathrust earthquake on 20 March 2012 was the only such event to occur during our study, so we investigated it for along-strike motion similar to how we analyzed the 2008-2009 SSE. We estimated site velocities from GPS data with the steady northeastward strain accumulation removed to accentuate any afterslip, for the first ~1.5 months after the 2012 Ometepec earthquake (Fig. S6). Fig. 7 shows that stations on the Xolapa terrane (OXTU, OXPE, OXLP) moved southeast while stations north of the terrane boundary (OXNC, OAX2, OXGU) moved southwest towards the afterslip patch. These motions are consistent with a combination of trenchward motion associated with afterslip on the megathrust and a-SSE on a crustal fault.

Graham et al. (57) who modeled the post-seismic deformation measured within 6 months of the 2012 Ometepec earthquake, found similar results with the exception of OXTU for which data was unavailable at the time. In fact, the along-strike motion for eastern sites on the Xolapa terrane do not fit well with the slip model in Graham et al. (57) suggesting afterslip on the plate interface cannot explain the along-strike motion at these stations. Furthermore, the downdip patch of afterslip (57) overlaps with the northern boundary of the Xolapa terrane indicating there could have been some slip on a strike-slip crustal fault. While we do not have a precise source location of the strike-slip motion, the observations are consistent with strike-slip motion on a crustal fault at the northern edge of the Xolapa terrane similar to the a-SSE observed during SSEs.

5. Discussion

Of the 14,000+ earthquakes in the local seismic catalog (OXNET), we found 404 (~3%) earthquakes within 20 swarms. Despite swarms only comprising 3% of the earthquake catalog, we believe they can provide valuable insight into subduction processes, in particular with regards to the region overlying the megathrust. Many of our swarms do not follow the dip of the plate

interface, instead consistent with a steeply dipping structure ~50-100 km inland from the trench (Fig. 4). In the central region where hypocenters are best constrained, the seismicity extends for over 20 km vertically, well beyond the depth uncertainty of 7 km (19). The horizontal trend of the swarms corresponds to a refined northern boundary of the Xolapa terrane based on the extent of the core complex (36), aeromagnetic data (20) and topographic information (22). GPS data indicate there are transient a-SSEs across this terrane boundary associated with SSEs and afterslip. In fact, swarms occurred during each of the a-SSEs during SSEs. Hence, these swarms and a-SSEs appear to be occurring on a steeply-dipping, strike-slip fault that represents the northern boundary of the Xolapa terrane.

Considering the angle of convergence in this portion of the Mexican Subduction Zone is slightly oblique relative to the trench (9-12^{o} in Guerrero and ~15^{o} in Oaxaca; (23)), we propose these swarms and a-SSEs represent the first documentation of sliver fault motion in Mexico (Fig. 8). The partitioning of oblique slip into trench perpendicular motion on the subduction interface and trench parallel motion on the sliver fault is not uncommon (58–60), and sliver faults have been seen in several regions, such as Kuril Arc (61, 62), Sumatra (63–65), El Salvador (66), and southern Chile (50, 67–70). The presence of a forearc sliver fault in Mexico may be driven in part by the flat slab configuration. According to a recent geodynamics study in southern Alaska, the Alaskan flat slab was found to drive the oblique motion of the Wrangell block forearc sliver, as there was strong plate coupling above the flat slab (71).

The nature of sliver fault motion in the form of earthquake swarms and a-SSEs has not been previously documented in other subduction zones. In particular, our observations indicate that transient slip during SSEs and afterslip is partitioned into trenchward dominant and along-strike dominant motion (i.e., a-SSEs) very close in time. The most similar scenario to our findings appears to be in southern Chile where the Liquiñe-Ofqui Fault Zone has been proposed to accommodate the forearc sliver motion associated with oblique subduction (72). There have been reported cases of swarms along the fault that have been attributed to both fluid-induced and tectonic processes where they could be a result of both (50, 51, 73). The proximity of the swarms to local volcanoes and the Liquiñe-Ofqui Fault Zone complicated determining which process was dominant. No SSEs have been reported for this region, perhaps due to limited resolving capability of cGPS in southern Chile. With the local cGPS and seismic network in Oaxaca and the absence of nearby volcanoes, we are able to better study the relationship between swarms and slow slip along a sliver fault associated with Mexico's oblique subduction.

Seismicity in the upper plate is not uncommon, but what is causing some of the seismicity to behave like swarms is a key question. Previous work has suggested slow slip is one of the possible driving mechanisms for earthquake swarms (9, 18, 74, 75). Along the plate interface, SSEs are thought to release trapped fluids from a low-permeability seal that forms in between episodes (47–49), which then flow upwards along the plate interface raising pore fluid pressures and lowering the effective stresses enough to generate seismicity (46, 76). The fluids are thought to have originated from the oceanic crust when blueschist dehydrates to eclogite, hence leading to the serpentinization of the overlying mantle wedge corner (77, 78). Therefore, the contrast in permeability between the impermeable gabbroic lower continental crust and the serpentinite below may trap fluids, contributing to high pore-fluid pressures and thus episodic tremor and slip generation (77, 79).

We propose a similar mechanism may be at play to generate swarms in Oaxaca but on the sliver fault rather than on the plate interface. The resistivity structure in Fig. 8 suggests that

swarms and a-SSEs occur due to high fluid content on or near the sliver fault. Arzate-Flores et al. (22) and Jödicke et al. (21) observed a zone of high conductivity at shallow depths close to the coast in Oaxaca which is believed to represent the presence of fluids. In the region overlying the plate interface updip of the episodic tremor and slip region, dehydrated-fluids are not trapped within the USL and are able to percolate into the overlying plate through fluid conduits, such as our proposed sliver fault during SSEs. Similarly, a recent study in Kanto, Japan found that seismicity rates and seismic attenuation above the plate interface changed following slow slip, suggesting slow slip releases trapped fluids that then migrate updip along the plate interface until they migrate into the overlying crust via an inherent permeable zone where they can trigger seismicity (80). Above the zone of high conductivity in southern Mexcio, Arzate-Flores et al. (22) found a more resistive zone which is believed to represent an impermeable silica layer that precipitates at 200ºC (81), thus trapping and over-pressurizing fluids released from the subducting crust. If the megathrust is well-drained, then the over-pressurized fluids that flow along crustal faults would facilitate shallow seismicity due to the consequent increase in pore-fluid pressures and decrease in the shear strength of the crustal faults (49, 82, 83) which would explain the occurence of our swarm seismicity and a-SSEs along the sliver fault. Even though results from Arzate-Flores et al. (22) are only along a single transect, we infer results extend out to include all swarms given that a zone of high conductivity near the coast is also seen further west in Guerrero (21) overlapping with the Xolapa terrane boundary (Fig. 1b).

If crustal faults are draining the megathrust, then the interaction between the sliver fault and dehydrated fluids could impact the downdip extent of the seismogenic zone. The rupture zone of the 2012 Ometepec earthquake (46) does not appear to extend past the sliver fault (Fig. 7) nor do previous megathrust ruptures (Fig. 8), indicating the fault may have some control on the downdip extent of seismogenic behavior. One possibility is that the sliver fault provides a pathway for buoyant fluids attempting to migrate upward after being released from the downgoing plate, as seen with other types of crustal faults ((84); and references therein). This creates drier conditions on the subduction interface trenchward of the sliver fault, promoting fast-slip seismogenic rupture behavior, whereas the presence of elevated pore-fluid pressures downdip result in slow rupture within the transition zone (85). In southern Chile, Moreno et al. (68) proposed that active crustal faults interacting with the plate interface should be considered when inverting geodetic data to constrain locking depths of the seismogenic zone. Estimating permeabilities along the sliver fault should be the focus of future work.

6. Conclusion

This study offers a new perspective on seismic and aseismic slip processes as well as crustal structures in the region overlying the megathrust. We compile a catalog of swarms in the Oaxaca region of southern Mexico that reveal a majority of the swarms form a steeply dipping structure in the overriding plate indicative of an origin other than the plate interface. Instead, the swarms appear to occur on the deeper extension of the regional Chacalapa-La Venta fault zone representing the northern boundary of the Xolapa terrane. This is supported by the fact that swarms occur during the later stages of SSEs when GPS site velocities shift from entirely trenchward dominant motion to components of along-strike dominant motion. Components of strike-slip motion across the Chacalapa-La Venta fault zone is also seen during afterslip of the 2012 Ometepec megathrust earthquake.

We propose the observations we have collected in this study are best explained by the Chacalapa-La Venta fault zone being a sliver fault accommodating slip partitioning associated with oblique subduction. The presence of a sliver fault could also explain a variety of previous observations, including: along-strike motion on coastal GPS sites in Guerrero (24, 40, 41); decrease in along-strike component of steady-state velocity moving inland (55, 56); unique rotational characteristic of slip before the 2006 SSE in Oaxaca, in addition to the times when there were small but significant eastward components at coastal sites (24). While sliver faults are not uncommon in oblique subduction zones, this study provides the first case of a sliver fault defined by swarms and slow slip. This could help explain why some sliver faults have been difficult to identify in the past and have been previously identified mainly based on GPS data of relative plate motions and slip vectors of megathrust earthquakes (62, 64, 66, 68, 72). We were able to identify the sliver fault in Mexico with a-SSEs and swarms, features not as common. Other regions with oblique convergence where a sliver fault has not been identified should be investigated for changes in direction of slow slip and swarm seismicity. The results would provide valuable information on how much of the partitioned trench parallel motion is released through seismic and aseismic slip.

Finally, we propose sliver faults may provide a conduit to drain fluids from the megathrust. Fluids released during dehydration are thought to be a primary factor in generating episodic tremor and slip along the deep end of the megathrust. Where those fluids travel to is a source of ongoing debate, but they could follow a subduction channel up into the seismogenic zone. A sliver fault could provide a permeability pathway that would divert fluid flow away from the shallow megathrust. Our observations of swarm behavior and slow slip on a sliver fault support this notion. Moreover, the sliver fault location coincides with the downdip end of the seismogenic zone, indicating a potential direct relationship.

Acknowledgements
Support for this work was provided by National Science Foundation grants EAR-1246944 (M.B.). O. Diaz-Molina and L. Salazar-Tlaczani were instrumental in establishing and maintaining the Oaxaca seismic network. This material is partly based on GPS data provided by the Trans-boundary Land and Atmosphere Long-term Observational and Collaborative Network (TLALOCNet) operated by UNAVCO and the Servicio de Geodesia Satelital from Instituto de Geofísica-UNAM and supported by NSF grant EAR-1338091, CONACyT project 253760 and UNAM-PAPIIT projects IN104213 and IN109315-3. Analyzed GPS time series is available upon request to the corresponding author. Personnel at Servicio de Geodesia Satelital-UNAM provided invaluable support for the TLALOCNet field operations, maintenance and data distribution.

References

1. Ruff LJ (1996) Large earthquakes in subduction zones: Segment interaction and recurrence times, in *Subduction: Top to Bottom* 96:91–104.
2. Dragert H, Wang KL, James TS (2001) A silent slip event on the deeper Cascadia subduction interface. *Science* 292:1525–1528.
3. Lowry A, Larson K, Kostoglodov V, Bilham R (2001) Transient slow slip in Guerrero, southern Mexico. *Geophys Res Lett* 28:3753–3756.

4. Ozawa S, et al. (2002) Detection and monitoring of ongoing aseismic slip in the Tokai region, Central Japan. *Science* 298:1009–1012.
5. Obara K (2002) Nonvolcanic deep tremor associated with subduction in southwest Japan. *Science* 296:1679–1681.
6. Rogers G, Dragert H (2003) Episodic tremor and slip on the Cascadia subduction zone: The chatter of silent slip. *Science* 300:1942–1943.
7. Szeliga W, Melbourne T, Miller M, Santillian V (2004) Southern Cascadia episodic slow earthquakes. *Geophys Res Lett* 31:L16602.
8. Shelly DR, Beroza GC, Ide S, Nakamula S (2006) Low-frequency earthquakes in Shikoku, Japan, and their relationship to episodic tremor and slip. *Nature* 442:188–191.
9. Ozawa S, Suito H, Tobita, M (2007) Occurrence of quasi-periodic slow-slip off the east coast of the Boso peninsula, Central Japan. *Earth Planets Space* 59:1241–1245.
10. Delahaye EJ, Townend J, Reyners ME, Rogers G (2009) Microseismicity but no tremor accompanying slow slip in the Hikurangi subduction zone, New Zealand. *Earth Planet Sci Lett* 277:21–28.
11. Vidale JE, Hotovec AJ, Ghosh A, Creager KC, Gomberg J (2011) Tiny intraplate earthquakes triggered by nearby episodic tremor and slip in Cascadia. *Geochem Geophys Geosyst* 12:Q06005.
12. Vallée M, et al. (2013) Intense interface seismicity triggered by a shallow slow slip event in the Central Ecuador subduction zone. *J Geophys Res Solid Earth* 118:2965–2981.
13. Ruiz S, et al. (2014) Intense foreshocks and a slow slip event preceded the 2014 Iquique Mw 8.1 earthquake. *Science* 345:1165–1169.
14. Poli P, Jeria AM, Ruiz S (2017) The Mw 8.3 Illapel earthquake (Chile): Preseismic and postseismic activity associated with hydrated slab structures. *Geology* 45:247–250.
15. Mogi K (1963) The fracture of a semi finite body caused by an inner stress origin and its relation to the earthquake phenomena. *Bull Earthq Res Inst* 41:615–658.
16. Sykes LR (1970) Earthquake swarms and sea-floor spreading. *J Geophys Res* 75:6598–6611.
17. Hill DP (1977) Model for earthquake swarms. *J Geophys Res* 82:1347–1352.
18. Holtkamp SG, Brudzinski MR (2011) Earthquake swarms in circum-Pacific subduction zones. *Earth Planet Sci Lett* 305:215–225.
19. Fasola S, et al. (2016) New perspective on the transition from flat to steeper subduction in Oaxaca, Mexico, based on seismicity, nonvolcanic tremor, and slow slip. *J Geophys Res Solid Earth* 121:1835–1848.
20. Ferrari L, Orozco-Esquivel T, Manea V, Manea M (2012) The dynamic history of the Trans-Mexican Volcanic Belt and the Mexico subduction zone. *Tectonophysics* 522:122–149.
21. Jödicke H, et al. (2006) Fluid release from the subducted Cocos plate and partial melting of the crust deduced from magnetotelluric studies in southern Mexico: Implications for the generation of volcanism and subduction dynamics. *J Geophys Res* 111:B08102.
22. Arzate-Flores JA, Molina-Garza R, Corbo-Camargo F, Márquez-Ramírez V (2016) Low angle contact between the Oaxaca and Juárez terranes deduced from magnetotelluric data. *Pure Appl Geophys* 173:3357–3371.
23. DeMets C, Gordon R, Argus D (2010) Geologically current plate motions. *Geophys J Int* 181:1–80.

24. Brudzinski M, Cabral-Cano E, Correa-Mora F, Demets C, Márquez-Azúa B (2007) Slow slip transients along the Oaxaca subduction segment from 1993 to 2007. *Geophys J Int* 171:523–538.
25. Correa-Mora F, DeMets C, Cabral-Cano E, Márquez-Azúa B, Diaz-Molina O (2008) Interplate coupling and transient slip along the subduction interface beneath Oaxaca, Mexico. *Geophys J Int* 175:269–290.
26. Correa-Mora F, DeMets C, Cabral-Cano E, Diaz-Molina O, Márquez-Azúa B (2009) Transient deformation in southern Mexico in 2006 and 2007: Evidence for distinct deep-slip patches beneath Guerrero and Oaxaca. *Geochem Geophys Geosyst* 10:Q02S12.
27. Brudzinski MR, et al. (2010) Nonvolcanic Tremor along the Oaxaca segment of the Middle America subduction zone. *J Geophys Res* 115: B00A23.
28. Graham SE, et al. (2014a) GPS constraints on the 2011–2012 Oaxaca slow slip event that preceded the 2012 March 20 Ometepec earthquake, southern Mexico. *Geophys J Int* 197:1593–1607.
29. Pardo M, Suárez G (1995) Shape of the subducted Rivera and Cocos plates in Southern Mexico: Seismic and tectonic implications. *J Geophys Res* 100:12357–12373.
30. Suárez G, Sánchez O (1996) Shallow depth of seismogenic coupling in southern Mexico: implication for the maximum size of earthquakes in the subduction zone. *Phys Earth Planet Inter* 93:53–61.
31. Pacheco JF, Singh SK (2010) Seismicity and state of stress in Guerrero segment of the Mexican subduction zone. *J Geophys Res* 115:B01303.
32. Pacheco JF, Sykes LR, Scholz CH (1993) Nature of seismic coupling along simple plate boundaries of the subduction type. *J Geophys Res* 98:14133–14159.
33. Tichelaar BW, Ruff LJ (1993) Depth of seismic coupling along subduction zones. *J Geophys Res* 98:2017–2037.
34. Suárez G, Monfret T, Wittlinger G, David C (1990) Geometry of subduction and depth of the seismogenic zone in the Guerrero gap, Mexico. *Nature* 345:336–338.
35. Ratschbacher L, Riller U, Meschede M, Herrmann U, Frisch W (1991) Second look at suspect terranes in southern Mexico. *Geology* 19:1233–1236.
36. Corona-Chávez P, Poli S, Bigioggero B (2006) Syn-deformational migmatites and magmatic-arc metamorphism in the Xolapa Complex, southern Mexico. *J Metamorph Geol* 24:169–191.
37. Riller U, Ratschbacher L, Frisch W (1992) Left-lateral transtension along the Tierra Colorada deformation zone, northern margin of the Xolapa magmatic arc of southern Mexico. *J South Am Earth Sci* 5: 237–249.
38. Tolson G (2005) La falla Chacalapa en el sur de Oaxaca. *Bol Soc Geol Mex* 57:111–122.
39. Solari LA, et al. (2007) Tectonic significance of Cretaceous-Tertiary magmatic and structural evolution of the northern margin of the Xolapa Complex, Tierra Colorada area, southern Mexico. *Geol Soc Am Bull* 119:1265–1279.
40. Yoshioka S, et al. (2004) Interplate coupling and a recent aseismic slow slip event in the Guerrero seismic gap of the Mexican subduction zone, as deduced from GPS data inversion using a Bayesian information criterion. *Phys Earth Planet Inter* 146:513–530.
41. Larson K, Kostoglodov V, Miyazaki S, Santiago JAS (2007) The 2006 aseismic slow slip event in Guerrero, Mexico: New results from GPS. *Geophys Res Lett* 34:L13309.

42. Song TA, et al. (2009) Subducting slab ultra-slow velocity layer coincident with silent earthquakes in Southern Mexico. *Science* 324:502–506.
43. Liu Y, Rice JR (2005) Aseismic slip transients emerge spontaneously in three-dimensional rate and state modeling of subduction earthquake sequences. *J Geophys Res* 110:B08307.
44. Liu Y, Rice JR (2007) Spontaneous and triggered aseismic deformation transients in a subduction fault model. *J Geophys Res* 112:B09404.
45. Rubinstein JL, et al. (2007) Nonvolcanic tremor driven by large transient shear stresses. *Nature* 448:579–582.
46. Colella HV, et al. (2017) Seismicity rate increases associated with slow slip episodes prior to the 2012 Mw 7.4 Ometepec earthquake. *Earth Planet Sci Lett* 464:35–45.
47. Audet P, Bostock MG, Christensen NI, Peacock SM (2009) Seismic evidence for overpressured subducted oceanic crust and sealing of the megathrust. *Nature* 45:76–78.
48. Audet P, Bostock MG, Boyarko DC, Brudzinski MR, Allen RM (2010) Slab morphology in the Cascadia forearc and its relation to episodic tremor and slip. *J Geophys Res* 115:B00A16.
49. Kato A, et al. (2010) Variations of fluid pressure within the subducting oceanic crust and slow earthquakes. *Geophys Res Lett* 37:L14310.
50. Lange D, et al. (2008) First seismic record for intra-arc strike-slip tectonics along the Liquiñe-Ofqui fault zone at the obliquely convergent plate margin of the Southern Andes. *Tectonophysics* 455:14–24.
51. Legrand D, Barrientos S, Bataille K, Cembrano J, Pavez A (2011) The fluid-driven tectonic swarm of Aysen Fjord, Chile (2007) associated with two earthquakes (Mw= 6.1 and Mw= 6.2) within the Liquiñe-Ofqui Fault Zone. *Cont Shelf Res* 31:154–161.
52. Kundu B, et al. (2012) The 2005 volcano–tectonic earthquake swarm in the Andaman Sea: Triggered by the 2004 great Sumatra–Andaman earthquake. *Tectonics* 31:TC5009.
53. Graham S, et al. (2016) Slow slip history for the Mexico subduction zone: 2005 through 2011. *Pure Appl Geophys* 173:3445–3465.
54. Vidale JE, Shearer PM (2006) A survey of 71 earthquake bursts across southern California: Exploring the role of pore fluid pressure fluctuations and aseismic slip as drivers. *J Geophys Res* 111:B05312.
55. Lowry AR, Larson KM, Kostoglodov V, Sanchez O (2005) The fault slip budget in Guerrero, southern Mexico. *Geophys J Int* 200:1–15.
56. Gaidzik K, Ramírez-Herrera MT, Kostoglodov V (2016) Active crustal faults in the forearc region, Guerrero sector of the Mexican subduction zone. *Pure Appl Geophys* 173:3419–3443.
57. Graham SE, et al. (2014b) GPS constraints on the M w= 7.5 Ometepec earthquake sequence, southern Mexico: coseismic and post-seismic deformation. *Geophys J Int* 199:200–218.
58. Fitch TJ (1972) Plate convergence, transcurrent faults, and internal deformation adjacent to southeast Asia and the western Pacific. *J Geophys Res* 77:4432–4460.
59. Jarrard RD (1986) Terrane motion by strike-slip faulting of forearc slivers. *Geology* 14:780–783.
60. McCaffrey R (1992) Oblique plate convergence, slip vectors, and forearc deformation. *J Geophys Res* 97:8905–8915.
61. Kimura G (1986) Oblique subduction and collision: Forearc tectonics of the Kuril arc. *Geology* 14:404–407.
62. DeMets C (1992) Oblique convergence and deformation along the Kuril and Japan trenches. *J Geophy Res* 97:17615–17625.

63. McCaffrey R (2009) The Tectonic Framework of the Sumatran Subduction Zone. *Annu Rev Earth Pl Sc* 37:345–366.
64. McCaffrey R, et al. (2000) Strain partitioning during oblique plate convergence in northern Sumatra: Geodetic and seismologic constraints and numerical modeling. *J Geophys Res* 105:28363–28376.
65. Berglar K, et al. (2010) Structural evolution and strike-slip tectonics off north-western Sumatra. *Tectonophysics* 480:119–132.
66. Corti G, Carminati E, Mazzarini F, Garcia MO (2005) Active strike-slip faulting in El Salvador, Central America. *Geology* 33:989–992.
67. Lange D, et al. (2007) Seismicity and geometry of the south Chilean subduction zone (41.5ºS–43.5ºS): Implications for controlling parameters. *Geophys Res Lett* 34:L06311.
68. Moreno MS, Klotz J, Melnick D, Echtler H, Bataille K (2008) Active faulting and heterogeneous deformation across a megathrust segment boundary from GPS data, south central Chile (36–39ºS). *Geochem Geophys Geosyst* 9:Q12024.
69. Melnick D, Bookhagen B, Strecker MR, Echtler H (2009) Segmentation of megathrust rupture zones from forearc deformation patterns over hundreds to millions of years, Arauco Peninsula. *J Geophys Res* 114:B01407.
70. Vargas G, et al. (2013) Submarine earthquake rupture, active faulting and volcanism along the major Liquiñe-Ofqui Fault Zone and implications for seismic hazard assessment in the Patagonian Andes. *Andean Geol* 40:141–171.
71. Haynie KL, Jadamec MA (2017) Tectonic drivers of the Wrangell block: Insights on fore-arc sliver processes from 3-D geodynamic models of Alaska. *Tectonics* 36:1180–1206.
72. Wang K, et al. (2007) Crustal motion in the zone of the 1960 Chile earthquake: Detangling earthquake‐cycle deformation and forearc‐sliver translation. *Geochem Geophys Geosyst* 8:Q10010.
73. Holtkamp SG, Pritchard ME, Lohman RB (2011) Earthquake swarms in South America. *Geophys J Int* 187:128–146.
74. Lohman RB, McGuire JJ (2007) Earthquake swarms driven by aseismic creep in the Salton Trough, California. *J Geophys Res* 112:B04405.
75. Wolfe CJ, Brooks BA, Foster JH, Okubo PG (2007) Microearthquake streaks and seismicity triggered by slow earthquakes on the mobile south flank of Kilauea Volcano, Hawaii. *Geophys Res Lett* 34:L23306.
76. Peng Z, Gomberg J (2010) An integrated perspective of the continuum between earthquakes and slow-slip phenomena. *Nat Geosci* 3:599–607.
77. Hyndman RD, McCrory PA, Wech A, Kao H, Ague J (2015) Cascadia subducting plate fluids channeled to fore-arc mantle corner: ETS and silica deposition. *J Geophys Res* 120:4344–4358.
78. Behr WM, Kotowski AJ, Ashley KT, (2018) Dehydration-induced rheological heterogeneity and the deep tremor source in warm subduction zones. *Geology* 46:475–478.
79. Audet P, Kim Y (2016) Teleseismic constraints on the geological environments of deep slow earthquakes in subduction zone fore arcs: A review. *Tectonophysics* 670:1–15.
80. Nakajima J, Uchida N (2018) Repeated drainage from megathrusts during episodic slow slip. *Nature Geoscience* 11:351–356.
81. Hyndman RD, Shearer PM (1989) Water in the lower continental crust: modelling magnetotelluric and seismic reflection results. *Geophys J Int* 98:343–365.

82. Sibson RH (2007) An episode of fault-valve behaviour during compressional inversion?—The 2004 M_J6. 8 Mid-Niigata Prefecture, Japan, earthquake sequence. *Earth Planet Sci Lett 257*:188–199.
83. Nakajima J, Hasegawa A (2016) Tremor activity inhibited by well-drained conditions above a megathrust. *Nature communications* 7:13863.
84. Saffer DM, Tobin HJ (2011) Hydrogeology and mechanics of subduction zone forearcs: Fluid flow and pore pressure. *Ann Rev Earth Planet Sci* 39:157–186.
85. Husker A, Ferrari L, Arango-Galván C, Corbo-Camargo F, Arzate-Flores JA (2018) A geologic recipe for transient slip within the seismogenic zone: Insight from the Guerrero seismic gap, Mexico. *Geology* 46:35–38.

Figures Legends

Fig. 1. Maps of Oaxaca, Mexico and surrounding regions. a) Map of various slip processes. Seismicity (OXNET catalog), amalgamation of SSEs, and region of tectonic tremor activity are represented by black dots, pink line, and purple line, respectively (19). Major earthquake rupture zones are outlined in blue. State boundaries are in white. b) Topographic map with approximate boundaries of lithologic terranes based on extent of core complexes (white lines; (20)). Terranes are abbreviated as CUICA, Cuicateco; GMP, Guerrero-Morelos platform; MIX, Mixteca; OAX, Oaxaca; XOL, Xolapa with La Venta Fault (LVF) and Chacalapa Fault (CF) labeled. Dashed white line marks old Xolapa-Mixteco boundary (20) for which we re-draw (solid white line)(see section S1.5). Location of seismic stations (triangles - inverted triangles are SSN) and cGPS (green squares, uppercase names) are shown. Straight black lines are profiles of magnetotelluric measurements with areas of high conductivity (>50 ohms) highlighted in yellow for Guerrero (21) and Oaxaca (22). Arrow indicates direction of relative plate motion (23).

Fig. 2. Magnitude vs. time for all earthquakes in swarms from June 2006 to March 2012 for Oaxaca and surrounding regions, colored by time.

Fig. 3. Map of seismicity in swarms colored by time as in Fig. 2. Boxes show areas of cross sections in Fig. 4. Slab depth contours are represented by solid black lines (19).

Fig. 4. Cross-sections of seismicity scaled by magnitude, oriented (a–c) downdip where the x-axis is the perpendicular distance inland from the trench. Dotted line represents approximation of the top of the slab (29). Events colored by time as in Fig. 2.

Fig. 5. Comparison of geodetic and swarm signatures. Black dots show GPS time series for OXTU trench perpendicular and trench parallel components. Pink boxes represent SSEs (46, 53) with trench perpendicular dominant motion and yellow boxes outline periods of along-strike dominant motion during the SSEs. Swarms (circles, colored as in Fig. 2) are plotted as magnitude vs. time.

Fig. 6. Comparison of March 10-19, 2009 swarm (circles, colored by time in (c)) and October 2008 - April 2009 SSE. a) Map of swarm and outline of cumulative slip (pink line, (53)). GPS velocities (arrows) represent an approximation of periods of trench pendicular dominant (pink) and trench parallel dominant (yellow) motions estimated from time series in (b) for each GPS

station (green squares). Black line represents line along which along-strike distances were determined in (c). b) Comparison of GPS time series (black circles) for coastal site OXTU and inland sites OXGU and OAX2 with a magnitude vs. time plot of the swarm. c) Time vs. Along-strike distance for the swarm. Black line represents our best-fit estimation of data for determining a migration rate.

Fig. 7. Map of March 20, 2012 Ometepec earthquake (light blue star) determined by the local network (46) and GPS velocities for post-seismic deformation ~1.5 months after the mainshock (green arrows) estimated from boxes in Fig. S5. Rupture zone and afterslip > 200 mm are marked by black striped circle (based on aftershocks from Colella et al. (46)) and green line (57), respectively, for the 2012 Ometepec earthquake.

Fig. 8. Diagram illustrating the occurrence of swarms (orange-striped circles) and along-strike slow slip (yellow circle) on a forearc sliver fault at the northern boundary of the Xolapa terrane. The face of the diagram shows a simplified version of the conductivity and density models from Arzate-Flores et al. (22) where cooler and warmer shades represent resistive and conductive regions, respectively. Lighter shades labeled with question marks are where we interpolated. The Xolapa, Mixteco, and Oaxaca terranes are shaded in gray based on a simplified version of the magnetic anomalies in Ferrari et al. (20) where dark gray and light gray represent a stronger and weaker magnetic anomaly, respectively. Black striped circles represent previous megathrust earthquakes.

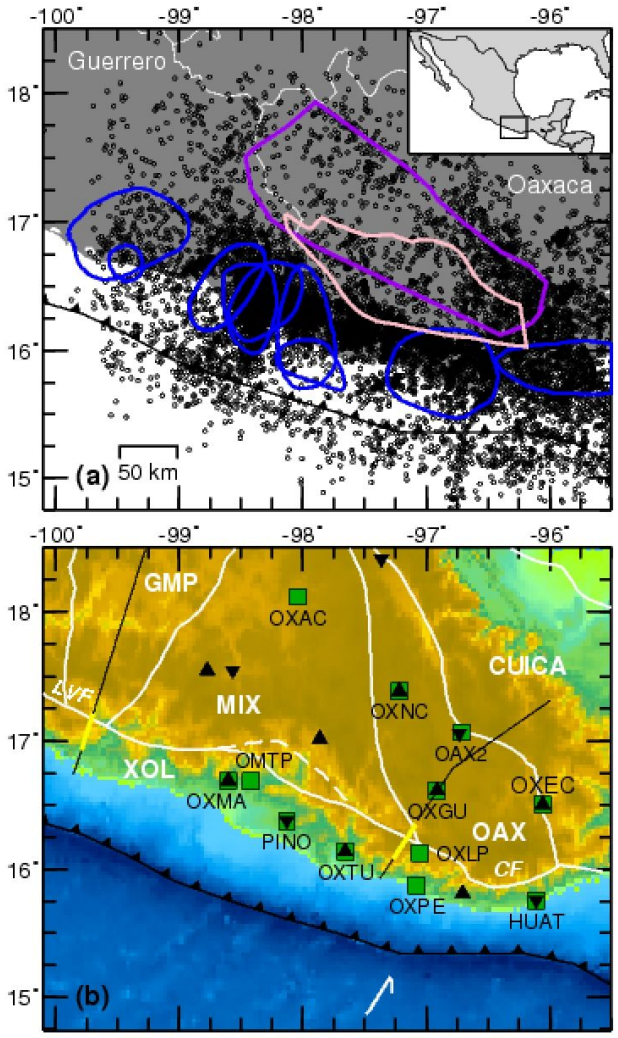

Figure 1.

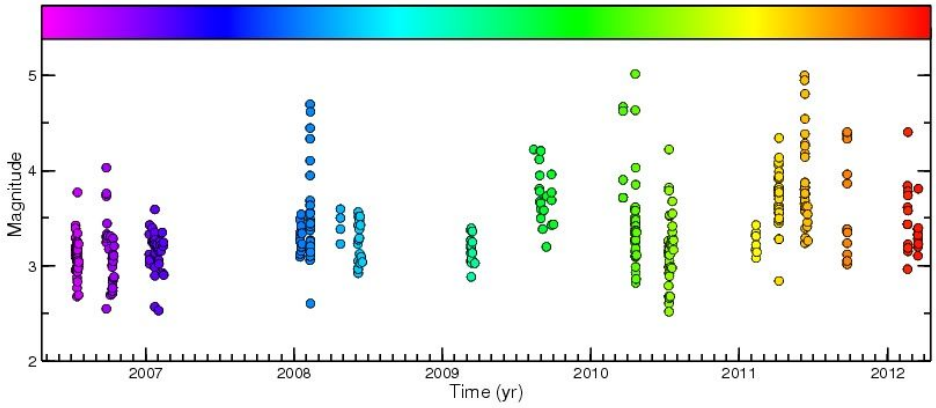

Figure 2.

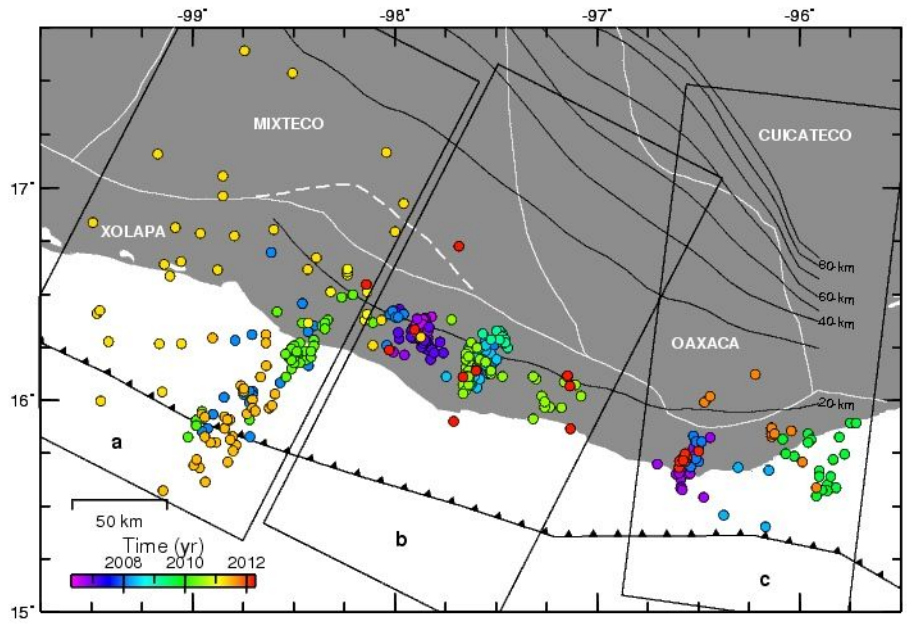

Figure 3.

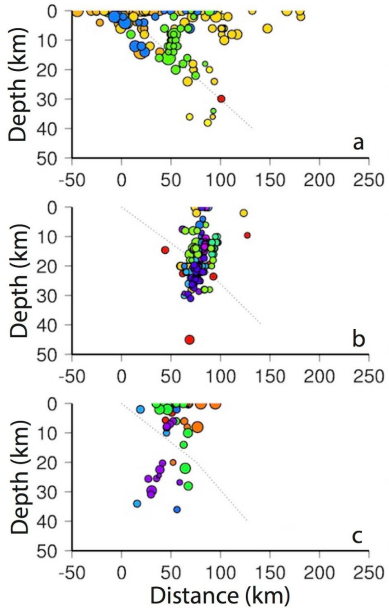

Figure 4.

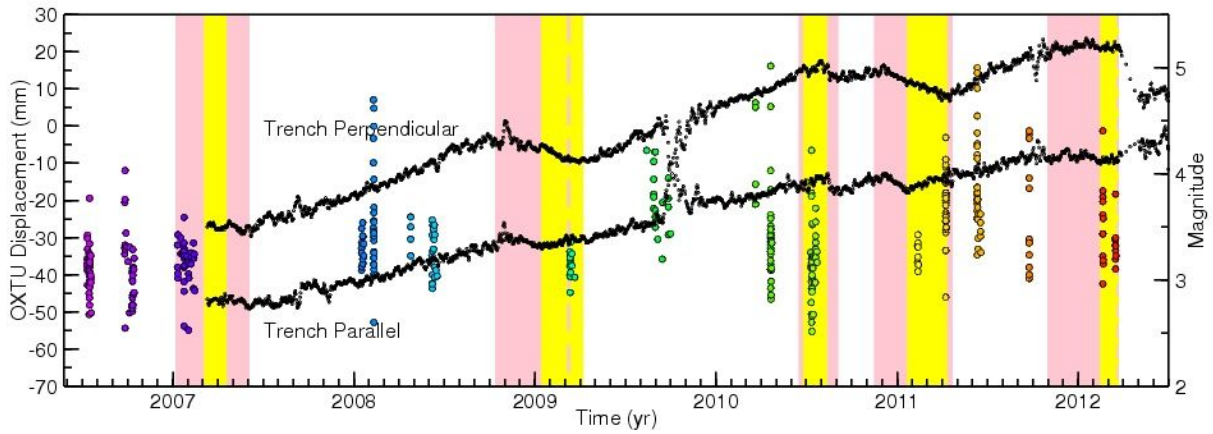

Figure 5.

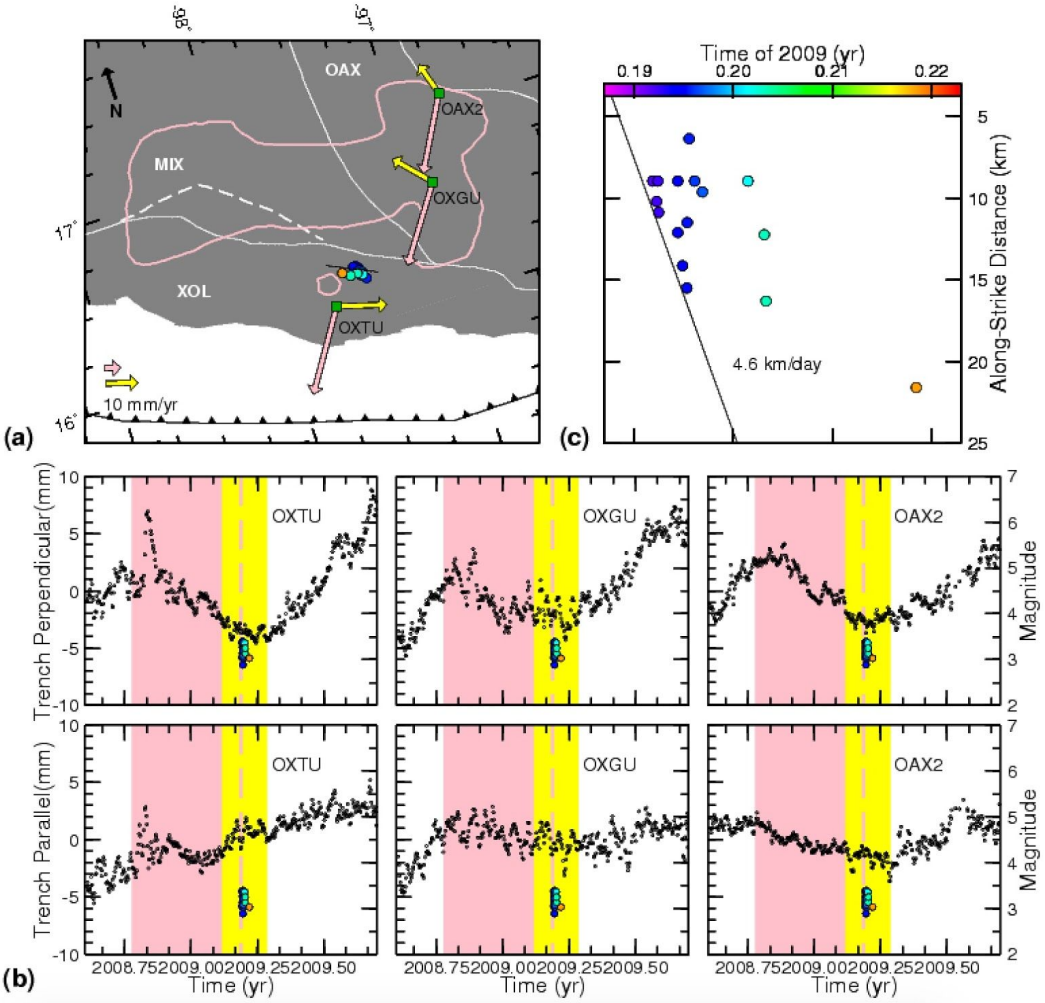

Figure 6.

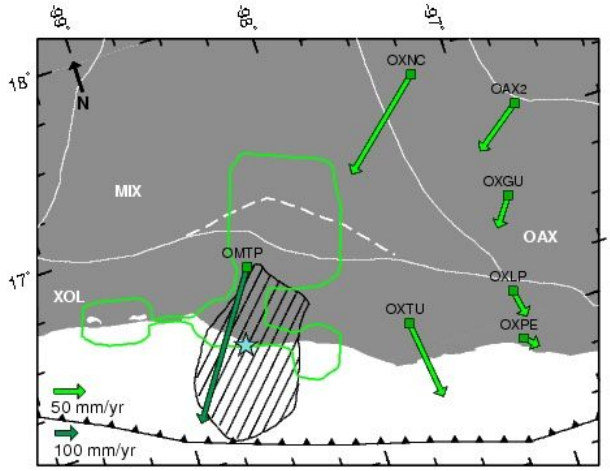

Figure 7.

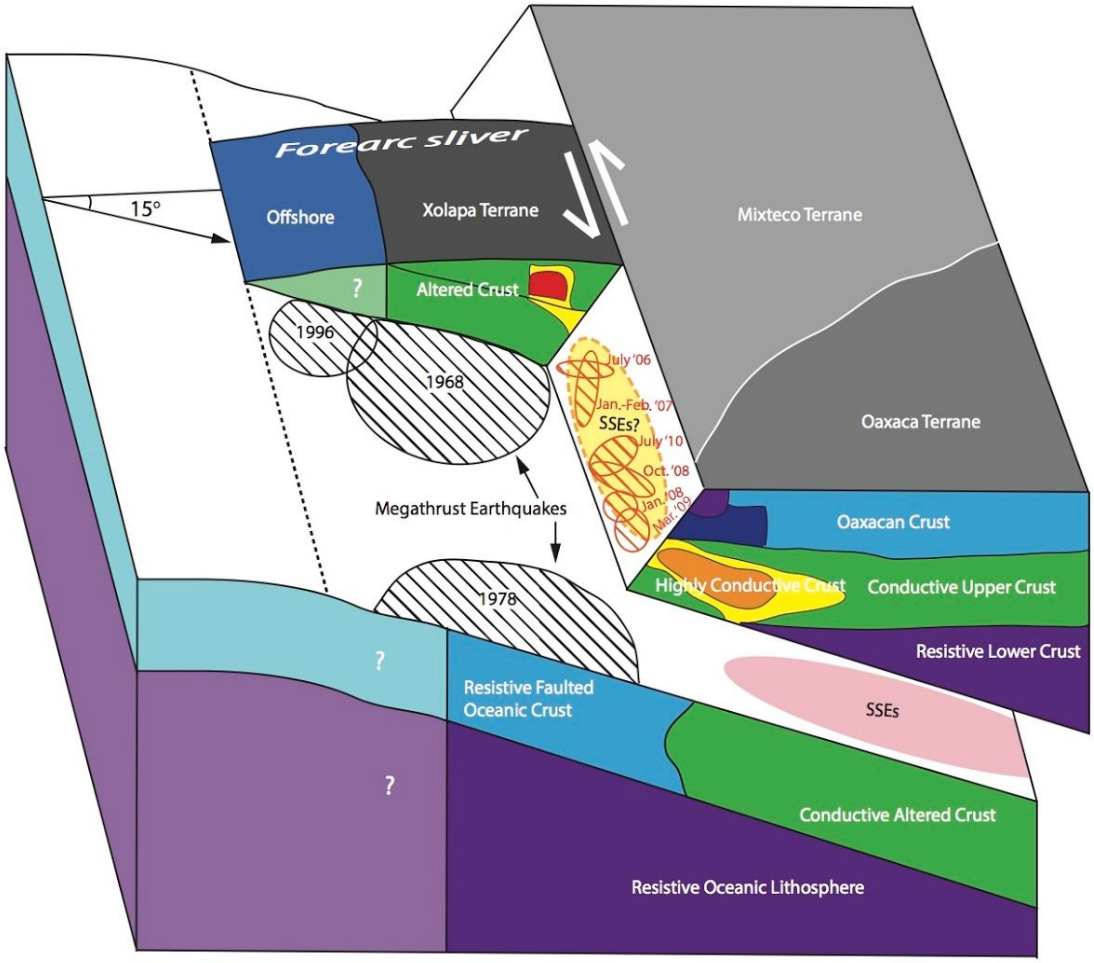

Figure 8.

Supporting Information

S1. Methods

S1.1. Seismic Data. All analyzed earthquakes are from the catalog of seismicity generated in Fasola et al. (1), referred to as the OXNET catalog. The catalog consists of 14,000+ earthquakes from June 2006 to March 2012, which were detected and located with the Antelope software package and a locally derived velocity model from Brudzinski et al. (2) modified from Valdes et al. (3). The detection of seismicity in the OXNET catalog utilized the local network of nine broadband seismometers in Oaxaca and eastern Guerrero in addition to five broadband seismic instruments (HUIG, PNIG, OXIG, TLIG, TPIG) from the National Seismological Service (SSN, Servicio Sismológico Nacional) array in Mexico. To help confirm the validity of magnitudes determined with Antelope, we compared the OXNET catalog with that of the SSN (http://www.ssn.unam.mx). Larger magnitudes tended to be overestimated by Antelope (Fig. S1), so we established a relationship to correct the magnitudes of the OXNET catalog.

S1.2. Swarm Identification. Using the swarm-characterization method of Holtkamp and Brudzinski (4), swarms are manually identified by visually inspecting every burst of seismicity that is constrained in space and time. Clusters of seismicity can be readily identified by the apparent line of vertical dots in a magnitude vs. time plot (Fig. 2). Those with a clear triggering mainshock were discarded while the remaining clusters were characterized by three empirical traits of swarm sequences: (1) no clear triggering mainshock, (2) many earthquakes near the maximum size (i.e., does not follow Bath's Law), and (3) a relatively constant rate of seismicity throughout the sequence (i.e., does not follow Omori's Decay Law) (Fig. S2). Earthquake swarms differ from mainshock-aftershock sequences (MSAS), in that MSAS the largest event is the first in the sequence after which the next largest event is typically one moment magnitude smaller (i.e., Bath's Law), and the rate of seismicity decays according to Omori's Law. We sought to use the OXNET catalog to characterize MSAS behavior by examining the sequences that follow all events M>3.5 with fewer than 5 events within 15 km in the prior week.

S1.3. Earthquake FMD. We calculated FMDs for swarms, the OXNET catalog, and the SSN catalog over the same time period (Fig. S3) following the Gutenberg-Richter *b*-value estimation of Bender (5):

$$b = 1/[\ln(10)\times(M_{avg} - (M_C - M_{bin}/2))]$$

where M_{avg} is the sampling average of the magnitudes, M_C is the magnitude of completeness, and M_{bin} is the bin size of earthquake magnitudes. M_C was determined using the maximum curvature algorithm (6). The resulting FMDs in Fig. S2 are generally similar for swarms, the OXNET catalog, and the SSN catalog, with slightly lower b-values for the swarms we identified.

S1.4. GPS data. We used data from 11 continuous GPS stations in Oaxaca spanning the duration of the OXNET catalog from June 2006 to March 2012. GPS data were processed with Release 6.1 of the GIPSY software suite from the Jet Propulsion Laboratory (JPL). No-fiducial daily GPS station coordinates were estimated using a precise point-positioning strategy (7), including constraints on a priori tropospheric hydrostatic and wet delays from Vienna Mapping Function (VMF1) parameters (http://ggosatm.hg.tuwien.ac.at), elevation- and azimuthally dependent GPS and satellite antenna phase center corrections from IGS08 ANTEX files (available via ftp from http://sideshow.jpl.nasa.gov), and corrections for ocean tidal loading

(http://holt.oso.chalmers.se). Phase ambiguities were resolved for all the data using GIPSY's single-station ambiguity resolution feature. The no-fiducial station location estimates were transformed to IGS08 using daily seven-parameter Helmert transformations from JPL, thereby yielding daily point-positioned station coordinates that conform to the International Terrestrial Reference Frame 2008 (ITRF08) (8). We applied methods described by Márquez-Azúa and DeMets (9) to estimate the common-mode noise for stations in southern Mexico and remove it from the position time series. Further details of this procedure are provided in Graham et al. (10). We did not solve for source locations of SSEs along the plate interface, as a catalog of SSEs in Oaxaca was recently compiled (11) utilizing the same GPS stations.

S1.5. Xolapa-Mixteco boundary. The Xolapa terrane is a crustal block that extends for 200 km along the coast from west of Acapulco to the Tehuantepec isthmus consisting of high-grade metamorphic rocks (Xolapa Metamorphic Complex) intruded by Tertiary plutons (12–15). We propose a small sector of the Xolapa-Mixteco boundary, to mimic the northern extent of the Xolapa Complex (15). This refined trajectory also mimics with the change in elevation as other studies have shown the Chacalapa-La Venta fault to coincide with the initial rise in elevation inland from the coast (16, 17) (Fig. 1b). Where the Xolapa-Mixteco boundary has been proposed to jut out inland, we instead propose the boundary continues along a straight path following the northern extent of the Xolapa Complex and base of the increase in elevation. This new interpretation better aligns with and follows the contrast in magnetic anomalies seen in Ferrari et al. (18) as we believe they suggest a change in composition (19) from the high-magnetic anomaly of the metamorphic and igneous Xolapa Complex (14, 15, 20–22) and the lower-magnetic anomaly of the deformed lower grade Mixteco Complex (23–26). In addition, our new path of the Xolapa-Mixteco boundary based on the extent of the core complex better aligns with the location of these newly detected earthquake swarms (Fig. 3) and our interpretation of a sliver fault.

S2. Confirmation and Characterization of Swarms

To confirm that the swarms we have identified follow the patterns of previous studies, we use the quantitative methods first suggested by Vidale and Shearer (27) that examined the relation of the largest event in each swarm and number of events in that swarm in addition to the relative timing of events within the swarm. Swarms tend to have a large number of events relative to the largest magnitude observed, relative to MSAS. This quantitative relationship matches a qualitative one: swarms are flurries of activity that do not have a signature large event. The distinction between this relationship for swarms and MSAS is seen in a plot of the largest earthquake in a cluster against the total number of earthquakes in that cluster. Fig. S4 shows a clear distinction between where swarms and MSAS sequences plot indicating that swarms are characteristically different from MSAS sequences. This distinction was seen in a variety of studies (4, 27–29).

In order to characterize the relative timing of events within the swarms, we used the time normalization method of Vidale and Shearer (27) where the timing of each event in a swarm was rescaled such that each swarm started at time 0 and had a mean time of 1. To compare the relative timing, we then summed the events of all 20 sequences (Fig. S5a). Similar to results of Vidale and Shearer (27), our results do not fit Omori-style rate functions. A key difference is seen between ~0.5-1.1 normalized time where the percentage of events is well above the

time-decay rate functions, uncharacteristic of MSAS sequences. ~15% of events are contained in the initial peak as in Vidale and Shearer (27). However, our results do not show a roughly constant rate of seismicity of ~5% following the initial burst as in Vidale and Shearer (27). Instead, our results show a more varied rate in seismicity which could be due to the smaller size of our swarm catalog. We also observed that the largest event in each sequence occurred at various times throughout the sequence indicating it is just another event and not always the initial event as in MSAS. For comparison, we looked at the temporal distribution of earthquakes within all MSAS with M>3.5 from the OXNET catalog (Fig. S5b). The MSAS sequences are a much better fit with the Omori-style rate functions with a greater percentage of events occurring in the initial time period. Even though our swarm catalog is smaller than Vidale and Shearer (27) and Holtkamp and Brudzinski (4), we still see similar characteristics in our swarms providing evidence that our catalog is in fact swarms.

When calculating b-values for our swarms, we found a b-value of 0.96, unexpected for swarms (Fig. S3a). Holtkamp and Brudzinski (4) found that swarms in circum-Pacific subduction zones typically have higher b-values (1.5 to 2) than the global Preliminary Determination of Epicenters (PDE) catalog (~1) indicating that swarms have less larger magnitude events compared to other earthquakes. In comparison, b-values for the OXNET and SSN catalogs were 1.13 and 1.19, respectively (Fig. S3b, c). These values are in agreement for typical seismicity.

Supporting Information Reference List

1. Fasola S, et al. (2016) New perspective on the transition from flat to steeper subduction in Oaxaca, Mexico, based on seismicity, nonvolcanic tremor, and slow slip. *J Geophys Res Solid Earth* 121:1835–1848.
2. Brudzinski MR, et al. (2010) Nonvolcanic tremor along the Oaxaca segment of the Middle America subduction zone. *J Geophys Res* 115:B00A23.
3. Valdes CM, et al. (1986) Crustal structure of Oaxaca, Mexico, from seismic refraction measurements. *Bull Seismol Soc Am* 76:547–563.
4. Holtkamp SG, Brudzinski MR (2011) Earthquake swarms in circum-Pacific subduction zones. *Earth Planet Sci Lett* 305:215–225.
5. Bender B (1983) Maximum likelihood estimation of b values for magnitude grouped data. *Bull Seismol Soc Am 73*:831–851.
6. Wiemer S, Wyss M (2000) Minimum magnitude of completeness in earthquake catalogs: Examples from Alaska, the western United States, and Japan. *Bull Seismol Soc Am* 90:859–869.
7. Zumberge JF, Heflin MB, Jefferson DC, Watkins MM, Webb FH (1997) Precise point positioning for the efficient and robust analysis of GPS data from large networks. *J Geophys Res* 102:5005–5018.
8. Altamimi Z, Collilieux X, Métivier L (2011) ITRF2008: an improved solution of the international terrestrial reference frame. *J Geodesy* 85:457–473.
9. Márquez-Azúa B, DeMets C (2003) Crustal velocity field of Mexico from continuous GPS measurements, 1993 to June 2001: Implications for the neotectonics of Mexico. *J Geophys Res* 108:2450.
10. Graham SE, et al. (2014a) GPS constraints on the 2011–2012 Oaxaca slow slip event that preceded the 2012 March 20 Ometepec earthquake, southern Mexico. *Geophys J Int* 197:1593–1607.

11. Graham S, et al. (2016) Slow slip history for the Mexico subduction zone: 2005 through 2011. *Pure Appl Geophys* 173:3445–3465.
12. Corona-Chávez P, Poli S, Bigioggero B (2006) Syn-deformational migmatites and magmatic-arc metamorphism in the Xolapa Complex, southern Mexico. *J Metamorph Geol* 24:169–191.
13. Schaaf P, et al. (1995) Paleogene continental margin truncation in southwestern Mexico: geo-chronological evidence. *Tectonics* 14:1339–1350.
14. Solari LA, et al. (2007) Tectonic significance of Cretaceous-Tertiary magmatic and structural evolution of the northern margin of the Xolapa Complex, Tierra Colorada area, southern Mexico. *Geol Soc Am Bull* 119:1265–1279.
15. Talavera-Mendoza O, et al. (2013) Origin and provenance of basement metasedimentary rocks from the Xolapa Complex: new constraints on the Chortise southern Mexico connection. *Earth Planet Sci Lett* 369:188–199.
16. Arzate-Flores JA, Molina-Garza R, Corbo-Camargo F, Márquez-Ramírez V (2016) Low angle contact between the Oaxaca and Juárez terranes deduced from magnetotelluric data. *Pure Appl Geophys* 173:3357–3371.
17. Gaidzik K, Ramírez-Herrera MT (2017) Geomorphic indices and relative tectonic uplift in the Guerrero sector of the Mexican forearc. *Geoscience Frontiers* 8:885–902.
18. Ferrari L, Orozco-Esquivel T, Manea V, Manea M (2012) The dynamic history of the Trans-Mexican Volcanic Belt and the Mexico subduction zone. *Tectonophysics* 522:122–149.
19. Purucker M, Whaler K (2007) Crustal magnetism. *Treatise Geophys* 5:195–237.
20. Herrmann UR, Nelson BK, Ratschbacher L (1994) The origin of a terrane: U/Pb zircon geochronology and tectonic evolution of the Xolapa complex (southern Mexico). *Tectonics* 13:455–474.
21. Ducea MN, et al. (2004) Rates of sediment recycling beneath the Acapulco trench: Constraints from (U-Th)/He thermochronology. *J Geophy Res* 109:B09404.
22. Pérez-Gutiérrez R, Solari LA, Gómez-Tuena A, Martens U (2009) Mesozoic geologic evolution of the Xolapa migmatitic complex north of Acapulco, southern Mexico: Implications for paleogeographic reconstructions. *Rev Mex Cienc Geol* 26:201–221.
23. Ortega-Gutiérrez F, Elías-Herrera M, Reyes-Salas M, Macías-Romo C, López R (1999) Late Ordovician–Early Silurian continental collision orogeny in southern Mexico and its bearing on Gondwana-Laurentia connections. *Geology* 27:719–722.
24. Keppie JD, et al. (2004) Implications of latest Pennsylvanian to Middle Permian paleontological and U-Pb SHRIMP data from the Tecomate Formation to re-dating tectonothermal events in the Acatlán Complex, southern Mexico. *Int Geol Rev* 46:745–753.
25. Talavera-Mendoza O, et al. (2005) U–Pb geochronology of the Acatlán Complex and implications for the Paleozoic paleogeography and tectonic evolution of southern Mexico. *Earth Planet Sci Lett* 235:682–699.
26. Nance RD, Miller BV, Keppie JD, Murphy JB, Dostal J (2006) Acatlán Complex, southern Mexico: Record spanning the assembly and breakup of Pangea. *Geology* 34:857–860.
27. Vidale JE, Shearer PM (2006) A survey of 71 earthquake bursts across southern California: Exploring the role of pore fluid pressure fluctuations and aseismic slip as drivers. *J Geophys Res* 111:B05312.

28. Holtkamp SG, Pritchard ME, Lohman RB (2011) Earthquake swarms in South America. *Geophys J Int* 187:128–146.
29. Skoumal RJ, Brudzinski MR, Currie BS (2015) Distinguishing induced seismicity from natural seismicity in Ohio: Demonstrating the utility of waveform template matching. *J Geophys Res Solid Earth* 120:6284–6296.

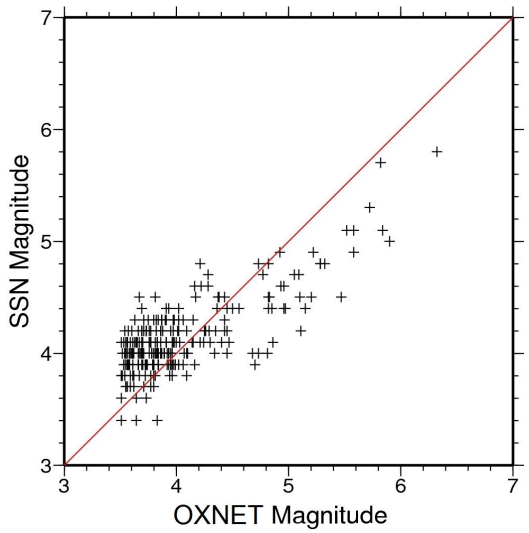

Fig. S1. Magnitudes of the OXNET catalog compared with magnitudes of the SSN catalog. We used a relationship to correct the OXNET magnitudes to match those of the SSN catalog:

$$M_{SSN} = 0.62 \times M_{OXNET} + 1.55$$

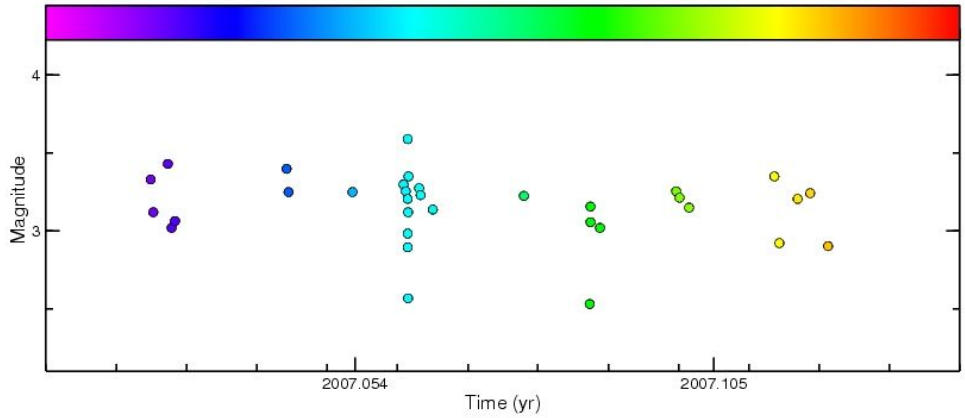

Fig. S2. Magnitude vs. time of a single swarm that lasted ~35 days in January 2007.

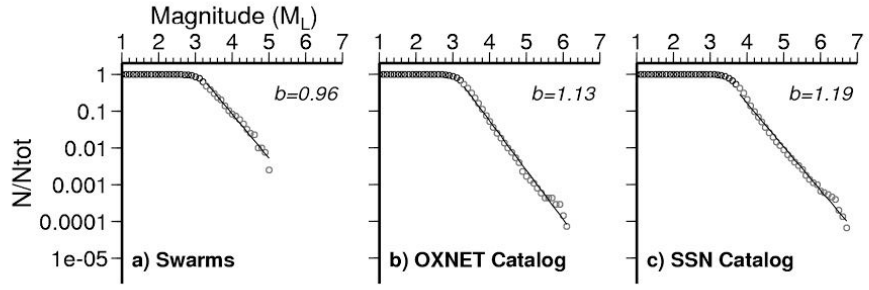

Fig. S3. Frequency-magnitude relationships for (a) all earthquakes within swarms and (b) all earthquakes in the OXNET catalog, (c) all earthquakes in the SSN catalog over the same time frame as the OXNET catalog. N/Ntot is the number of events at or above a given magnitude divided by the total number of events. b is the log-linear slope of the frequency-magnitude relation.

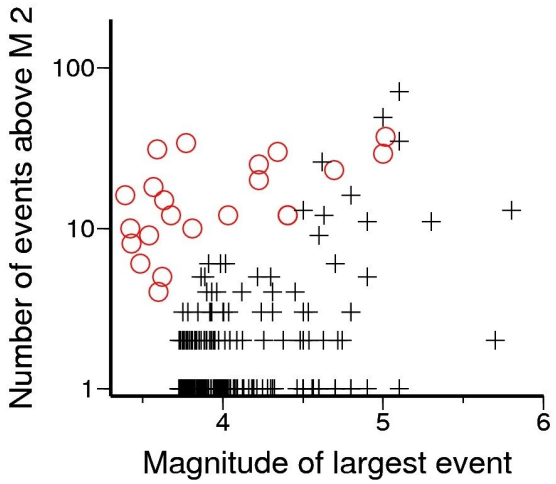

Fig. S4. Number of earthquakes in a sequence above a magnitude 2 relative to the magnitude of the largest earthquake in that sequence. Red circles are the swarms from this study and the black crosses are the MSAS sequences for all events above a magnitude 3.5 from the OXNET catalog.

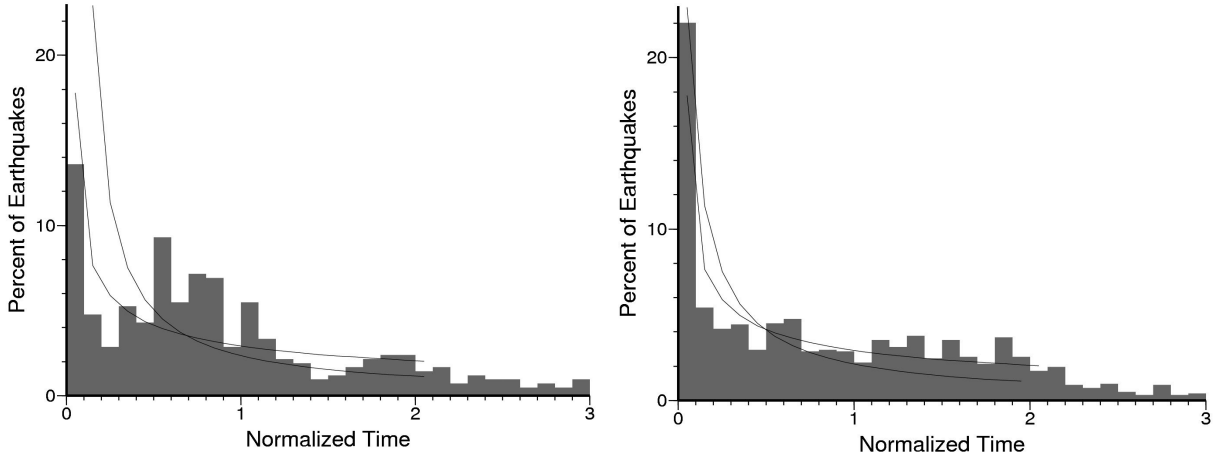

(a) Swarms (b) MSAS

Fig. S5. (a) Relative timing of earthquakes within all swarms where the timing is normalized to the total duration of each swarm with a mean time of 1 and then all 20 swarms are stacked together. Timing is normalized following Vidale and Shearer (27). (b) Relative timing of earthquakes in MSAS with M>3.5 from the OXNET catalog with time normalized and events stacked as in (a). Black lines are two Omori-type rate functions.

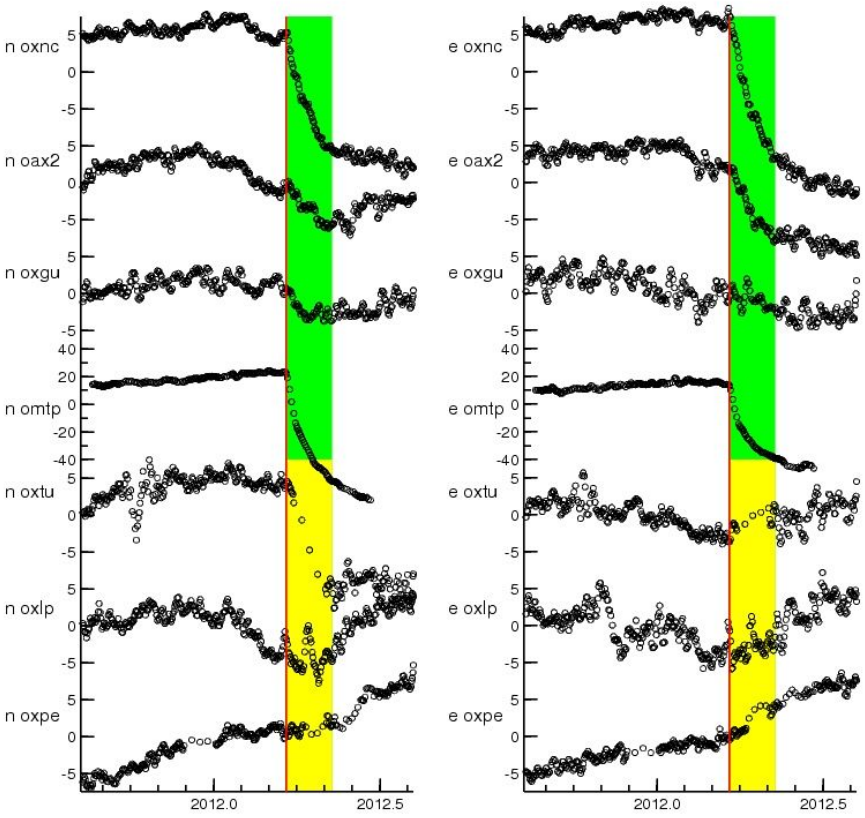

Fig. S6. GPS time series highlighting afterslip 1.5 months following the 2012 Ometepec earthquake (red line) for which GPS velocities were calculated in Fig. 7. Green and yellow boxes represent stations with afterslip in the trenchward and along-strike directions, respectively.